Stress-Induced High-T_c Superconductivity in Solid Molecular Hydrogen

Xianqi Song[a,1], **Chang Liu**[a,b,c,1], **Quan Li**[a,b,c,2], **Russell J. Hemley**[d,2], **Yanming Ma**[a,b,2], **and Changfeng Chen**[e,2]

[a]State Key Lab of Superhard Materials and International Center for Computational Method and Software, College of Physics, Jilin University, Changchun 130012, China; [b]International Center of Future Science, Jilin University, Changchun 130012, China; [c]Jilin Provincial International Cooperation Key Laboratory of High-Efficiency Clean Energy Materials, Jilin University, Changchun 130012, China; [d]Departments of Physics, Chemistry, and Earth and Environmental Sciences, University of Illinois Chicago, Chicago, Illinois 60607, USA; [e]Department of Physics and Astronomy, University of Nevada, Las Vegas, Nevada 89154, USA

This manuscript was compiled on March 14, 2022

Solid molecular hydrogen has been predicted to be metallic and high-temperature superconducting at ultrahigh hydrostatic pressures that push current experimental limits. Meanwhile, little is known about the influence of non-hydrostatic conditions on its electronic properties at extreme pressures where anisotropic stresses are inevitably present and may also be intentionally introduced. Here we show by first-principles calculations that solid molecular hydrogen compressed to multimegabar pressures can sustain large anisotropic compressive or shear stresses which, in turn, cause major crystal symmetry reduction and charge redistribution that accelerate bandgap closure and promote superconductivity relative to pure hydrostatic compression. Our findings highlight a hitherto largely unexplored mechanism for creating superconducting dense hydrogen, with implications for exploring similar phenomena in hydrogen-rich compounds and other molecular crystals.

high pressure | anisotropic stresses | metallic hydrogen | superconductivity | first-principles calculations

Since Wigner and Huntington's pioneering work (1), pressure-induced metallization of hydrogen has attracted immense interest and impelled advances of theoretical and computational methods, ultrahigh-pressure devices, and related measurement and characterization techniques (2, 3). The prediction (4) that metallic hydrogen may be a high-temperature superconductor driven by the BCS-type phonon-mediated mechanism further invigorated the study of this fascinating material and its enigmatic properties. As a prominent thermodynamic quantity, pressure, which is defined as hydrostatic, drives the formation of new material phases through structural transitions and electronic bandgap closure (5). Two main avenues have been pursued for producing metallic hydrogen at high pressure: (i) closure of the electronic bandgap of solid molecular hydrogen and (ii) dissociation of hydrogen molecules to form monatomic metal. These mechanisms have been explored through optical and electrical conductivity techniques over the years (6–16). In addition, at least five molecular phases, labeled I−V, have been documented experimentally to pressures up to 400 GPa and temperatures 300 K (17–21). These very high static pressures can significantly limit, constrain, and challenge full experimental characterization of materials, especially above 300 GPa, leading to ambiguities and controversies in the interpretation of reported results.

Theoretical studies (22–27) of the metallization of solid hydrogen have focused on its formation under hydrostatic pressure. However, conditions inside diamond anvil cells (DACs) at the required pressures (e.g., >300 GPa) can introduce nonuniform deformations and anisotropic stresses in the vicinity of the sample as revealed by direct x-ray imaging study above 300 GPa (28). More recent studies have further explored these effects (29, 30) and have also unveiled unprecedented structural ductility in diamond under large multiaxial deformation modes (31, 32), underscoring complex strain conditions inside DACs under extreme loading conditions. It is therefore instructive to establish the influence of anisotropic stresses on the evolution of structural and electronic properties of molecular hydrogen under nonhydrostatic pressure conditions [More discussion of non-hydrostatic stress states in DACs can be found in the Supporting Information (SI)]. Although gases that are solidified under pressure are often assumed to be hydrostatic over a range of pressures, direct measurements indicate the development of anisotropic strains even well below 100 GPa (33). Moreover, significant pressure gradients were documented even in the earliest optical studies of closing of the bandgap above 200 GPa (2, 7).

Here we report an exploratory study of metallization and superconductivity of solid molecular hydrogen under anisotropic stresses, i.e., at non-hydrostatic pressures. Our first-principles stress-strain calculations establish that despite being a soft and plastic crystal at low pressures (and temperatures) solid hydrogen at megabar pressures can sustain considerable uniaxial compressive and shear stresses, and such anisotropic stresses can have major impact on physical properties. Promi-

Significance Statement

Metallic hydrogen has long been considered the Holy Grail of high pressure physics that holds the intriguing possibility of realizing room-temperature superconductivity. However, the ultrahigh pressures required for hydrogen metallization impose severe experimental challenges and constraints on synthesis and characterization, leaving large ambiguities and controversies in the interpretation of reported results. We show that non-hydrostatic stresses offer a viable route to promote metallization and superconductivity in hydrogen at more accessible static compression conditions (e.g., <300 GPa). Such stress anisotropy is expected to be highly dependent on sample and measurement conditions, which may explain the discrepancies in previously reported experimental results, including variations in the rate of bandgap closure and onset of electrical conductivity in solid molecular hydrogen.

Q.L., R.J.H., Y.M., and C.C. designed the research; X.S. and C.L. performed the calculations; X.S., C.L., Q.L., R.J.H., Y.M., and C.C. analyzed the data and wrote the paper.

The authors declare no competing interest.

[1]X.S. and C.L. contributed equally to this work.

[2]To whom correspondence should be addressed. E-mail: liquan777@jlu.edu.cn, rhemley@uic.edu, mym@jlu.edu.cn, or changfeng.chen@unlv.edu

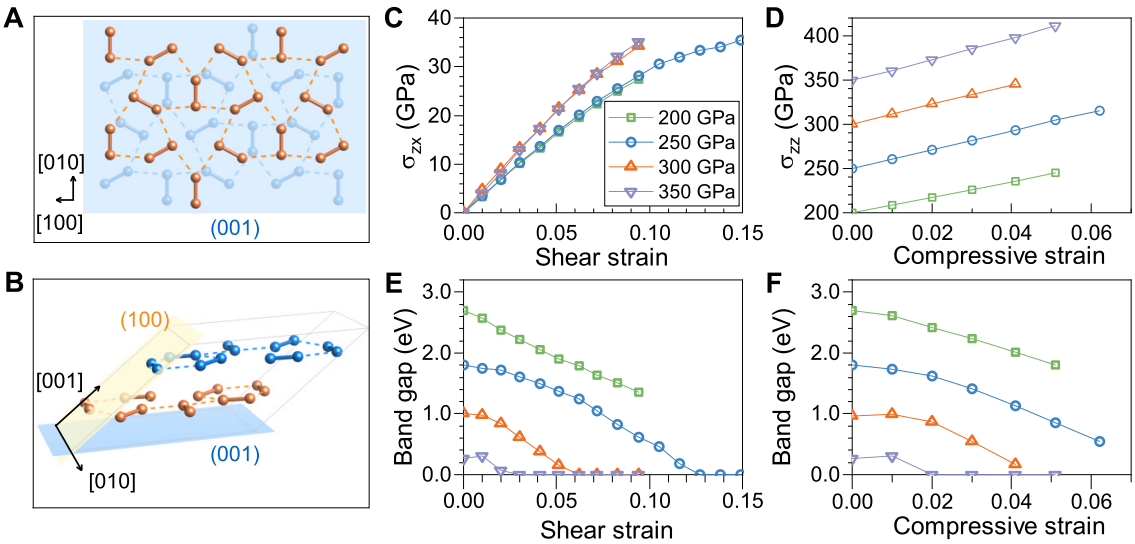

Fig. 1. Structure and stress and bandgap responses of solid molecular hydrogen to anisotropic stresses. (A) Top and (B) polyhedral view of the $C2/c$ phase. The thick solid lines represent the intramolecular covalent bonds of H_2 and the thin dash lines are intermolecular links. The light grey lines outline the unit cell. (C) First-principles determined stable stress responses to shear strains along the (010)[001] direction (the loading path with the steepest descent of E_g) at hydrostatic pressures of 200, 300, and 350 GPa and along the (001)[010] direction (the loading path with the easiest metallization of E_g) at 250 GPa. (D) First-principles determined stable stress responses to compressive strains in the [100] direction at 200, 250, 300, and 350 GPa. (E and F) Shear and compressive strain-modified E_g along the above selected loading paths.

nent effects include lattice symmetry reduction and ensuing changes in the electronic band structure that accelerate the bandgap closure, leading to metallization, and enhance the electron-phonon coupling (EPC) giving rise to superconductivity. In particular, we find that shear deformations are highly effective in inducing metallic and superconducting states at much reduced hydrostatic pressures. These phenomena are driven by robust underpinning mechanisms and are therefore expected to remain intact when possible corrections by thermal and quantum effects are further considered. The present findings may explain loading-dependent differences in reported experimental results (9–16, 34, 35) and show that introducing controlled non-hydrostatic stresses is a viable route to promote metallization and superconductivity in hydrogen at readily accessible static compression conditions (e.g., <300 GPa).

Stress responses and bandgap evolution of solid molecular hydrogen. To explore the impact of anisotropic stresses on the transition of solid hydrogen from insulating to metallic and potentially high-T_c superconducting states, we focus on phase III of solid hydrogen, which was discovered in 1988 (2, 6) and has been predicted and observed to be the stable insulating phase at temperatures below 200 K in the pressure range of about 150-400 GPa before potentially turning metallic upon further compression. The extremely high pressures required to achieve metallization has been a formidable challenge to reliable measurements and analysis. Theoretical calculations (17, 36) for phase III have predicted two nearly degenerate thus coexisting structures of $C2/c$ symmetry containing 12 and 24 atoms per unit cell, respectively, which are compatible with the low-temperature Raman and infrared (IR) spectra (36). In this work, we focus on the $C2/c$-12 structure (see Fig. 1 A and B) as an exemplary case study; our studies show that this phase is able to sustain large anisotropic stresses and more easily transform into metallic states. We first performed extensive first-principles calculations to determine the stress responses of the $C2/c$ structure to anisotropic compression and shear strains in the hydrostatic pressure range of 200-350 GPa, and key representative stress responses are summarized in Fig. 1 C and D (full stress-strain relations are given in *SI Appendix* Figs. S1 and S2 and crystal structure information of representative deformed molecular hydrogen is listed in *SI Appendix* Table S1). It is seen that the structure can sustain considerable anisotropic compressive stresses ranging from 30 to 60 GPa that increase with rising hydrostatic pressure of 200-350 GPa or shear stresses of about 30 GPa that are insensitive to hydrostatic pressure.

Electronic band-structure calculations show that these non-hydrostatic stresses that give rise to anisotropic strains lower the bandgap E_g relative to the equivalent isotropic stresses or hydrostatic pressures (see *SI Appendix* Fig. S3) as shown in Fig. 1 E and F), stemming from band shifts and splittings caused by the symmetry reduction of the deformed crystal. In particular, we find that shear strains ε_{zx} are highly effective in reducing E_g; for instance, a shear stress σ_{zx}=20 GPa at ε_{zx} =0.06 along the (010)[001] direction reduces E_g at hydrostatic pressure of 200 GPa to approximately E_g at 250 GPa. Remarkably, a shear stress $\sigma_{zx} = 33$ GPa along the (001)[010] direction causes a complete bandgap closure at 250 GPa (see Fig. 1E), which occurs at 370 GPa under hydrostatic conditions. At higher pressures, bandgap closure occurs at smaller shear strains, as shown in Fig. 1E for selected cases (see *SI Appendix* Fig. S1 for more comprehensive results).

We also examine the evolution of E_g with excess uniaxial compressive strain (ε_{zz}) added to compressive strains induced by hydrostatic pressure. The results show a reduction of E_g at the rate of about 20 meV/GPa ($\Delta E_g/\Delta\sigma_{zz} = 0.9$ eV/45 GPa), which is greater than 16 meV/GPa ($\Delta E_g/\Delta P = 2.4$ eV/150 GPa) of E_g reduction under hydrostatic pressure (see Fig. 1 D and F). The metallization can be realized at 350 GPa by introducing an additional normal compressive stress of about 23 GPa. Additional results on the compressive stress-strain and corresponding E_g-strain relations presented in *SI Appendix*

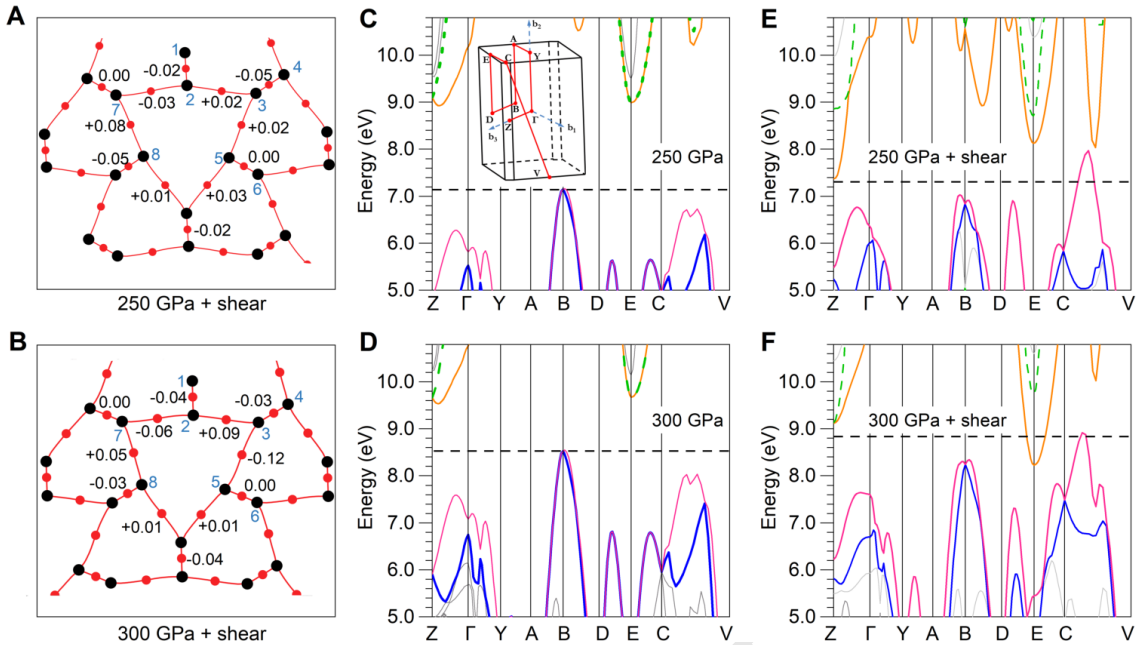

Fig. 2. Electronic properties of shear deformed $C2/c$ hydrogen. (A and B) QTAIM analysis of charge states in the (001) plane of shear deformed $C2/c$-based structure at 250 GPa and 300 GPa. The large (small) black (red) spheres represent hydrogen atoms and bond critical points (BCPs), respectively. The change of charge density for BCPs is given in the atom unit. (C and D) Electronic band structures at the hydrostatic pressure of 250 GPa and 300 GPa. The inset shows the Brillouin zone path for calculating the band structures. (E and F) Electronic band structures of shear deformed $C2/c$-based structure at σ_{zx}=35 GPa (ε_{zx}=0.149) in the (001)[010] direction at 250 GPa and at σ_{zx}=34 GPa (ε_{zx}=0.094) in the (010)[001] direction at 300 GPa. The black dashed lines mark the Fermi energy. The bands are colored to exhibit band shifts and splits.

Fig. S2 indicate that anisotropic compressive stresses can also play a role but are less effective compared with shear stresses in inducing the metallization.

Shear-induced metallization of molecular hydrogen. To further elucidate the appreciable modifications of electronic properties in non-hydrostatic environments, we performed a quantum theory of atoms in molecules (QTAIM) analysis of changes of charge states in response to stress-induced structural variations. We examine the bonding structures and charge density at bond critical points (BCPs) to evaluate the bonding strength and charge transfer. When hydrostatic pressure increases from 250 GPa to 300 GPa, the charge density values at the BCPs of the hydrogen molecules remain unchanged (2.07 to 2.07 and 2.12 to 2.12) and the values between hydrogen molecules rise by about 0.08 a.u. (0.62 to 0.70, 0.61 to 0.69, and 0.59 to 0.67) (see *SI Appendix* Fig. S4 for more details), implying almost constant bond length of H_2 molecules and increased intermolecular interactions, producing pressure-induced energy-band broadening and E_g decrease (see Fig. 2 *C* and *D*). Shear deformation drives intramolecular charge delocalization and differential evolution of hydrogen atomic distance (see *SI Appendix* Fig. S5 *a* and *b*) while enhancing intermolecular interactions and breaks the degeneracy of electronic states due to symmetry reduction. The change of charge density at BCPs of the $C2/c$ structure under combined hydrostatic pressure of 250 GPa and shear stress of $\sigma_{zx} = 35$ GPa ($\varepsilon_{zx} = 0.149$) in the (001)[010] direction (see Fig. 2*A*) shows an in-plane charge transfer from intramolecular to intermolecular regions (the distance of H7-H8 from 1.190 Å to 1.134 Å, H3-H5 from 1.190 Å to 1.171 Å), weakening the intramolecular bonds, elongating the H_2 units, and resulting in hole-type bands (see Fig. 2*E*). Meanwhile, shear deformation causes the growth of charge distribution in the interlayer region under shear strains in the (010)[001] direction at 300 GPa (see Fig. 2*B*) with decreasing interlayer spacing (the distance of H3-H5 from 1.145 Å to 1.260 Å). The antibonding states of H_2 molecules start to be filled, lowering the conduction band minimum, producing the electron-type band crossing at the Fermi energy, and mediating an indirect band gap closure (see Fig. 2*F*).

Superconductivity in shear-deformed molecular hydrogen. There have been extensive theoretical studies of potentially very high-T_c superconductivity in molecular hydrogen induced by hydrostatic compression (37–39). The present work expands such studies by introducing additional tuning mechanisms via anisotropic stresses, which drives metallization of the molecular solid at considerably reduced pressures. We further examine superconductivity of solid molecular hydrogen under shear strains along the easiest metallization paths in the (001)[010] direction at 250 GPa and the (010)[001] direction at 300 GPa. We find enhanced electron-phonon coupling under shear strains. To expose the underlying mechanism, we have calculated the phonon dispersion relations and the Eliashberg spectral function (see Fig. 3). Major contributions to the electron-phonon coupling parameter λ come from the low-frequency branches (acoustic phonons and librons) around 10−20 THz corresponding to the translational and rotational motions of the H_2 molecules. The phonons characterize the centers-of-mass molecular motions and the librons correspond to coupled restricted rotations (40). The distinguishable high-frequency vibrons are coupled stretchy vibrations of the H_2 molecules; notably these give rise to large peaks in the Eliashberg spectral function $\alpha^2F(\omega)$ at some q points but the high phonon frequency ω limits their contributions to the electron-phonon coupling parameter. For the (001)[010] shear loading

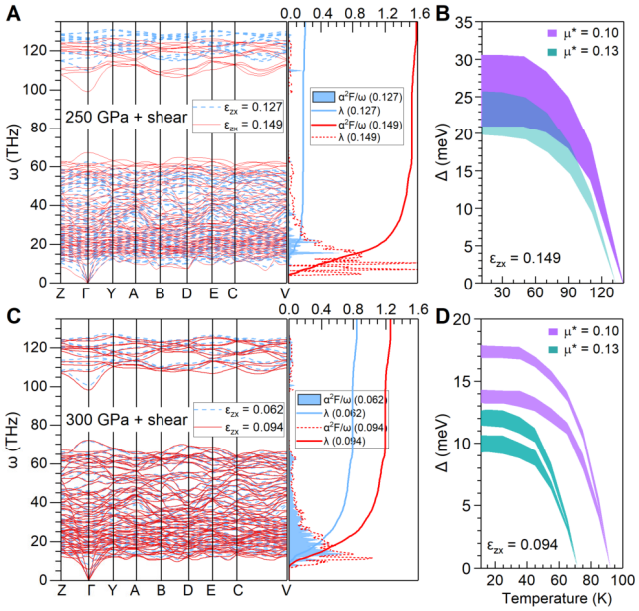

Fig. 3. Shear-induced superconductivity in $C2/c$ hydrogen. (A) Phonon dispersion relations ω(k) and Eliashberg spectral function α^2F(ω)/ω and $\lambda(\omega)$ at σ_{zx}=33 GPa (ε_{zx}=0.127) and σ_{zx}=35 GPa (ε_{zx}=0.149) and (B) the anisotropic superconducting gap (Δ) and superconducting critical temperatures (T_c) at shear strain ϵ_{zx}=0.149 in the (001)[010] direction at 250 GPa. (C) Phonon dispersion relations ω(k) and Eliashberg spectral function α^2F(ω)/ω and $\lambda(\omega)$ at σ_{zx}=25 GPa (ε_{zx}=0.062) and σ_{zx}=34 GPa (ε_{zx}=0.094) and (D) the anisotropic superconducting gap (Δ) and T_c at shear strain ε_{zx}=0.094 in the (010)[001] direction at 300 GPa.

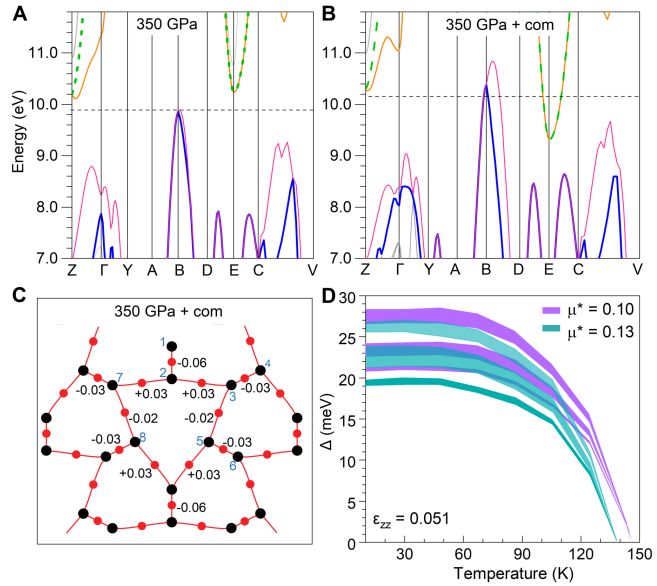

Fig. 4. Electronic properties of $C2/c$ hydrogen under anisotropic strain at 350 GPa. (A and B) Electronic band structures at 350 GPa and at σ_{xx}=σ_{yy}=350 GPa, σ_{zz}=411 GPa (ε_{zz}=0.051) in the [100] direction. The black dashed lines mark the Fermi energy. The bands are colored to exhibit band shifts and splits. (C) The structure and charge density based on QTAIM analysis of $C2/c$ hydrogen under conditions in (B). (D) The corresponding superconducting gap (Δ) and T_c.

path at 250 GPa, the in-plane charge transfers from the intramolecular to intermolecular regions, which weakens the covalent diatomic molecular bonds and softening the vibrons, reducing the intermolecular repulsion, and softening the librons (see Fig. 3*A*). Meanwhile, the hole-type band crosses the Fermi energy along the Brillouin zone path C→V (see *SI Appendix* Fig. S6 *a* and *b*), producing superconducting critical temperatures (T_c) of 132 K (μ^*=0.13) to 140 K (μ^*=0.10) at shear strain σ_{zx}=0.149 (see Fig. 3*B*). For the (010)[001] shear loading path at 300 GPa, the incremental accumulation of interlayer electrons with rising strains contributes to the electron-phonon coupling at ε_{zx}=0.094 by initiating new topologies of the Fermi surface (see *SI Appendix* Fig. S6 *c* and *d*) and softening phonons (see Fig. 3*C*). The change produces a two-gap superconducting state stemming from the anisotropic and varied Fermi surface structures with a T_c of 72 K (μ^*=0.13) to 93 K (μ^*=0.10) (see Fig. 3*D*).

Molecular hydrogen under anisotropic compressive strains. We also examined $C2/c$ hydrogen under anisotropic compressive strains at 350 GPa (see Fig. 4). The degeneracy of the conduction band remains intact, but the conduction band minimum drops as in the shear-deformed cases (see Fig. 4 *A* and *B*). In contrast to the hydrostatic and shear-strain cases, the bond lengths of the hydrogen molecules increase here (see *SI Appendix* Fig. S5*c*), indicating more intramolecular electron transfer to the intermolecular (in-plane and interlayer) regions, in agreement with the charge density analysis of BCPs from QTAIM (see Fig. 4*C*). These new charge states produce complex band characteristics and Fermi surfaces (see *SI Appendix* Fig. S6 *e* and *f*), resulting in a multigap superconducting state with T_c of 138 K (μ^*=0.13) to 145 K (μ^*=0.10) at ε_{zz}=0.051 under the anisotropic compressive stress conditions σ_{xx}= σ_{yy}=350 GPa and σ_{zz}=411 GPa (see Fig. 4*D*).

Discussion

First-principles calculations of stress-strain relations indicate that phase III of solid hydrogen can sustain large anisotropic stresses at megabar pressures, and the accompanying reversible deformations in the elastic region notably alter the crystal symmetry, charge distributions, and bonding behavior. The resulting band shifts, splittings, and enhanced electron-phonon coupling of the phase can dramatically exceed those induced by pure isotropic compression. The effects lead to band gap closure and ensuing superconductivity at significantly reduced compressive stresses compared to hydrostatic conditions. Most notable is shear deformation causing hydrogen to become metallic and superconducting at 250 GPa, which is about 120 GPa (i.e., >30%) lower than that obtained under hydrostatic conditions predicted at the same level of calculation. These results provide specific predictions that could be tested on hydrogen under extreme compression by additional stress conditions that are achievable in the laboratory. Since such stress anisotropy is in general highly sample and P-T path dependent, the present results may help to explain apparent discrepancies in previously reported experimental results, including variations in rate of bandgap closure and onset of electrical conductivity in solid molecular hydrogen (7, 8, 10–12). Furthermore, stress anisotropy in such compressed materials can be both controlled (e.g, by varying the geometry of thin samples and thermal annealing) and can be measured with various spectroscopic, diffraction, and imaging techniques (28, 29, 33).

We now comment on possible impact of quantum and thermal effects on the present findings. It has been proposed that the prototypical quantum crystal, low-density solid ^{4}He,

may develop giant nonclassical plasticity (41), but it was also pointed out that the observed phenomenon may be primarily rooted in thermal rather than quantum effects (42), and a later study showed (43) that the stress responses are well described by classical mechanical theory. Moreover, strength enhancement of solid helium under pressure has been documented (44), and analogous results were observed in hydrogen (45). Experimental studies of other low Z systems, such as Li, LiH and LiF, document significant contributions of both thermal (e.g., Debye-Waller) effects and quantum zero-point effects on their lattice dynamics (46, 47). For phase III of hydrogen, anharmonic finite-temperature effects have been shown to reduce the electronic band gaps (48). The quantum nature of the protons and anharmonicity are also predicted to increase the intramolecular distance and enhance superconductivity in molecular hydrogen (49). Thermal effects tend to soften crystals and reduce compressive and shear strengths (50), but probably do not have a large influence on the structural and mechanical behavior at the pressure-temperature regimes of interest here (>200 GPa and <300 K).

In conclusion, this study opens a new avenue and perspective on the metallization and potential high-T_c superconductivity in dense hydrogen under stress conditions possible in high-pressure experiments, most notably static compression studies using diamond anvil cells. The results provide an instructive comparison to many benchmark theoretical studies of molecular hydrogen, i.e., as a classical crystal at the same level of theory under hydrostatic pressures (13, 21–25, 27, 37–39) versus the nonhydrostatic conditions considered in this work. While quantum and thermal effects may modify some predicted quantitative aspects, these effects are not expected to change the trends and alter our principal conclusions about the impact of anisotropic stresses on the electronic properties of hydrogen under pressure. Moreover, the findings have implications for other molecular solids and related systems, which are likely to sustain even higher shear stresses than dense solid hydrogen. These materials include hydride high Tc superconductors (34, 35, 51–54), whose stability ranges and properties may be significantly altered by anisotropic stresses.

Materials and Methods

We have performed the structural relaxation and stress-strain relation calculations using the Vienna Ab-initio Simulation Package (VASP) code, adopting the projector-augmented wave method and the GGA-PBE exchange-correlation functional (XC) with 900 eV cutoff energy and $8 \times 9 \times 10$ Monkhorst-Pack k-mesh. The stress-strain relations are determined with a strain increment of 0.01, where at each step the applied the shear or compressive strain is fixed to determine the shear stress σ_{xz} or compressive stress σ_{zz}, respectively, while the other five independent components of the strain tensors and all atomic positions are simultaneously relaxed. The vdW-DF2 XC has been used to calculate the bandgap E_g, electronic band structure, and Fermi surface of molecular hydrogen implemented in VASP code. We have used the quantum theory of atoms in molecules (QTAIM) analysis implemented in AIM-UC software. The lattice dynamics and electron-phonon coupling calculations were performed using the QUANTUM ESPRESSO code, adopting an energy cutoff of 80 Ry and an $8 \times 8 \times 8$ k mesh and $4 \times 4 \times 4$ q mesh (see *SI Appendix* Fig. S7 for the convergence test). The anisotropic superconducting gap and T_c are calculated using the open-source electron-phonon Wannier code. More computational details can be found in the Supporting Information.

Data Availability. All study data are included in this article and/or SI Appendix.

ACKNOWLEDGMENTS. This work was supported by the National Key Research and Development Program of China under Grant No. 2021YFA1400503, the Natural Science Foundation of China under Grants No. 52090024, No. 12074140 and No. 12034009, the US National Science Foundation (DMR-1933622), the US DOE/NNSA (DE-NA0003975), and the Program for the JLU Science and Technology Innovative Research Team. The reported calculations utilized computing facilities at the High-Performance Computing Center of Jilin University. This paper is dedicated to the 70th anniversary of the physics program at Jilin University.

1. E. Wigner, H. B. Huntington, On the possibility of a metallic modification of hydrogen. *J. Chem. Phys.* **3**, 764-770 (1935).
2. H. K. Mao, R. J. Hemley, Ultrahigh-pressure transitions in solid hydrogen. *Rev. Mod. Phys.* **66**, 671-692 (1994).
3. J. M. McMahon, M. A. Morales, C. Pierleoni, D. M. Ceperley, The properties of hydrogen and helium under extreme conditions. *Rev. Mod. Phys.* **84**, 1607–1653 (2012).
4. N. W. Ashcroft, Metallic Hydrogen: a high-temperature superconductor?. *Phys. Rev. Lett.* **21**, 26 (1968).
5. L. J. Zhang, Y. C. Wang, J. Lv, Y. M. Ma, Materials discovery at high pressures. *Nat. Rev. Mater.* **2**, 17005 (2017).
6. R. J. Hemley, H. K. Mao, Phase transition in solid molecular hydrogen at ultrahigh pressures. *Phys. Rev. Lett.* **61**, 857 (1988).
7. H. K. Mao, R. J. Hemley, Optical studies of hydrogen above 200 gigapascals: evidence for metallization by band overlap. *Science* **244**, 1462-1465 (1989).
8. C. Narayana, H. Luo, J. Orloff, A. L. Ruoff, Solid hydrogen at 342 GPa: no evidence for an alkali metal. *Nature* **393**, 46-49 (1998).
9. A. F. Goncharov, E. Gregoryanz, R. J. Hemley, H. K. Mao, Spectroscopic studies of the vibrational and electronic properties of solid hydrogen to 285 GPa. *Proc. Natl. Acad. Sci. U.S.A.* **98**, 14234-14237 (2001).
10. P. Loubeyre, F. Occelli, R. LeToullec, Optical studies of solid hydrogen to 320 GPa and evidence for black hydrogen. *Nature* **416**, 613-617 (2002).
11. M. I. Eremets, I. A. Troyan, Conductive dense hydrogen. *Nat. Mater.* **10**, 927-931 (2011).
12. C. S. Zha, Z. Liu, R. J. Hemley, Synchrotron infrared measurements of dense hydrogen to 360 GPa. *Phys. Rev. Lett.* **108**, 146402 (2012).
13. A. F. Goncharov *et al.*, Bonding, structures, and band gap closure of hydrogen at high pressures. *Phys. Rev. B* **87**, 024101 (2013).
14. R. P. Dias, I. F. Silvera, Observation of the Wigner-Huntington trantision to metallic hydrogen. *Science* **355**, 715-718 (2017).
15. M. I. Eremets, A. P. Drozdov, P. P. Kong, H. Wang, Semimetallic molecular hydrogen at pressure above 350 GPa. *Nat. Phys.* **15**, 1246-1249 (2019).
16. P. Loubeyre, F. Occelli, P. Dumas, Synchrotron infrared spectroscopic evidence of the probable transition to metal hydrogen. *Nature* **577**, 631-635 (2020).
17. C. J. Pickard, R. J. Needs, Structure of phase III of solid hydrogen. *Nat. Phys.* **3**, 473-476 (2007).
18. C. J. Pickard, M. Martinez-Canales, Density functional theory study of phase IV of solid hydrogen. *Phys. Rev. B* **85**, 214114 (2012).
19. J. McMinis, R. C. Clay III, D. Lee, M. A. Morales, Molecular to atomic phase transition in hydrogen under high pressure. *Phys. Rev. Lett.* **114**, 105305 (2015).
20. P. Dalladay-Simpson, R. T. Howie, E. Gregoryanz, Evidence for a new phase of dense hydrogen above 325 gigapascals. *Nature* **529**, 63-67 (2016).
21. B. Monserrat *et al.*, Structure and metallicity of phase V of hydrogen. *Phys. Rev. Lett.* **120**, 255701 (2018).
22. M. A. Morales, J. F. McMahon, C. Pierleoni, D. M. Ceperley, Towards a predictive first-principles description of solid molecular hydrogen with density functional theory. *Phys. Rev. B* **87**, 184107 (2013).
23. I. I. Naumov, R. E. Cohen, R. J. Hemley, Graphene physics and insulator-metal transition in compressed hydrogen. *Phys. Rev. B* **88**, 045125 (2013).
24. R. Singh, S. Azadi, T. D. Kuhne, Anharmonicity and finite-temperature effects on the structure, stability, and vibrational spectrum of phase III of solid molecular hydrogen. *Phys. Rev. B* **90**, 014110 (2014).
25. S. Azadi, N. D. Drummond, W. M. C. Foulkes, Nature of the metallization transition in solid hydrogen. *Phys. Rev. B* **95**, 035142 (2017).
26. W. L. Yim, H. L. Shi, Y. F. Liang, R. J. Hemley, J. S. Tse, Band gaps and effective oscillator models for solid hydrogen and H_2O ice at high pressure. in *Correlations in Condensed Matter under Extreme Conditions* (eds. G. G. N. Angilella and A. La Magna), 107-126 (World Scientific, 2017).
27. L. Monacelli, I. Errea, M. Calandra, F. Mauri, Black metal hydrogen above 360 GPa driven by proton quantum fluctuations. *Nat. Phys.* **17**, 63-67 (2021).
28. R. J. Hemley *et al.*, X-ray imaging of stress and strain of diamond, iron, and tungsten at megabar pressures. *Science* **276**, 1242-1245 (1997).
29. B. Li *et al.*, Diamond anvil cell behavior up to 4 Mbar. *Proc. Natl. Acad. Sci. USA* **115**, 1713-1717 (2018).
30. V. I. Levitas, M. Kamrani, B. Feng, Tensorial stress-strain fields and large elastoplasticity as well as friction in diamond anvil cell up to 400 GPa. *npj Comput. Mater.* **5**, 94 (2019).
31. C. Liu, X. Q. Song, Q. Li, Y. M. Ma, C. F. Chen, Smooth flow in diamond: atomistic ductility and electronic conductivity. *Phys. Rev. Lett.* **123**, 195504 (2019).
32. Z. Shi *et al.*, Metallization of diamond. *Proc. Natl. Acad. Sci. USA* **117**, 24634-24639 (2020).
33. H. K. Mao, J. Badro, J. Shu, R. J. Hemley, A. K. Singh, Strength, anisotropy, and preferred orientation of solid argon at high pressures. *J. Phys. Condens. Matter* **18**, S963 (2006).
34. M. Somayazulu *et al.*, Evidence for superconductivity above 260 K in lanthanum superhydride at megabar pressures. *Phys. Rev. Lett.* **122**, 027001 (2019).
35. A. P. Drozdov *et al.*, Superconductivity at 250 K in lanthanum hydride under high pressures.

Nature **569**, 528-531 (2019).
36. J. S. Tse, D. D. Klug, Y. S. Yao, Y. L. Page, J. R. Rodgers, Structure and spectroscopic properties of dense solid hydrogen at 160 GPa. *Solid State Commun.* **145**, 5-10 (2008).
37. L. J. Zhang *et al.*, *Ab initio* prediction of superconductivity in molecular metallic hydrogen under high pressure. *Solid State Commun.* **141**, 610-614 (2007).
38. P. Cudazzo *et al.*, *Ab initio* description of high-temperature superconductivity in dense molecular hydrogen. *Phys. Rev. Lett.* **100**, 257001 (2008).
39. P. Cudazzo *et al.*, Electron-phonon interaction and superconductivity in metallic molecular hydrogen. II. Superconductivity under pressure. *Phys. Rev. B* **81**, 134506 (2010).
40. P. Cudazzo *et al.*, Electron-phonon interaction and superconductivity in metallic molecular hydrogen. I. Electronic and dynamical properties under pressure. *Phys. Rev. B* **81**, 134505 (2010).
41. A. Haziot, X. Rojas, A. D. Fefferman, J. R. Beamish, S. Balibar, Giant plasticity of a quantum crystal. *Phys. Rev. Lett.* **110**, 035301 (2013).
42. C. Zhou, C. Reichhardt, M. J. Graf, J.-J. Su, Comment on "Giant plasticity of a quantum crystal". *Phys. Rev. Lett.* **111**, 119601 (2013).
43. E. J. L. Borda, W. Cai, M. de Koning, Ideal shear strength of a quantum crystal. *Phys. Rev. Lett.* **112**, 155303 (2014).
44. C. S. Zha, H. K. Mao, R. J. Hemley, Elasticity of dense helium. *Phys. Rev. B* **70**, 174107 (2004).
45. C. S. Zha, T. S. Duffy, H. K. Mao, R. J. Hemley, Elasticity of hydrogen to 24 GPa from single-crystal Brillouin scattering and synchrotron x-ray diffraction. *Phys. Rev. B* **48**, 9246 (1993).
46. C. Sternemann *et al.*, Influence of lattice dynamics on electron momentum density of lithium. *J. Phys. Chem. Solids* **61**, 379 (2000).
47. G. Dolling, H. G. Smith, R. M. Nicklow, P. R. Vijayaraghavan, M. K. Wilkinson, Lattice Dynamics of Lithium Fluoride. *Phys. Rev.* **168**, 970 (1968).
48. R. Singh, S.m Azadi, T. D. Kühne, Anharmonicity and finite-temperature effects on the structure, stability, and vibrational spectrum of phase III of solid molecular hydrogen. *Phys. Rev. B* **90**, 014110 (2014).
49. M. Borinaga *et al.*, Anharmonic enhancement of superconductivity in metallic molecular Cmca-4 hydrogen at high pressure: a first-principles study. *J. Phys. Condens. Matter* **28**, 494001 (2016).
50. L. Wen, H. Wu, H. Sun C. F. Chen, Profound softening and shear-induced melting of diamond under extreme conditions: An ab-initio molecular dynamics study. *Carbon* **155**, 361-368 (2019).
51. H. Wang, J. S. Tse, K. Tanaka, T. Iitaka, Y. M. Ma, Superconductive sodalite-like clathrate calcium hydride at high pressures. *Proc. Natl. Acad. Sci. USA* **109**, 6463-6466 (2012).
52. F. Peng *et al.*, Hydrogen clathrate structures in rare earth hydrides at high pressures: possible route to room-temperature superconductivity. *Phys. Rev. Lett.* **119**, 107001 (2017).
53. H. Y. Liu, I. I. Naumov, R. Hoffmann, N. W. Ashcroft, R. J. Hemley, Potential high-T_c superconducting lanthanum and yttrium hydrides at high pressures. *Proc. Natl. Acad. Sci. USA* **114**, 6990-6995 (2017).
54. E. Snider *et al.*, Room-temperature superconductivity in a carbonaceous sulfur hydride. *Nature* **586**, 373-377 (2020).